Journal of Applied Electrochemistry (2006) 36:1391–1397
DOI 10.1007/s10800-006-9222-z

Electrocatalytic oxidation of ethanol on Pt–Mo bimetallic electrodes in acid medium

D.M. DOS ANJOS[1], K.B. KOKOH[1,*], J.M. LÉGER[1], A.R. DE ANDRADE[2], P. OLIVI[2] and G. TREMILIOSI-FILHO[3]
[1]*Equipe Electrocatalyse, UMR 6503, CNRS - Université de Poitiers - 40, Avenue du Recteur Pineau, 86022, Poitiers Cedex, France*
[2]*Departamento de Química, Faculdade de Filosofia, Ciências e Letras de Ribeirão Preto, Universidade de São Paulo, 14040-901, Ribeirão Preto, SP, Brazil*
[3]*Instituto de Química de São Carlos, Universidade de São Paulo, 13560-970, São Carlos, SP, Brazil*
*(*author for correspondence, fax: + 33-549-45-35-80, e-mail: boniface.kokoh@univ-poitiers.fr)*

Received 1 January 2006; accepted in revised form 15 August 2006

Key words: Pt–Mo catalyst, ethanol, electrooxidation, Mo dissolution

Abstract

Pt–Mo alloy electrocatalysts were prepared by an arc-melting furnace process to investigate the origin of their enhanced activity toward ethanol oxidation. Two Mo contents were chosen in zones of the binary phase diagram where they are supposed to form either a pure alloy mixture or a solid solution. Pt–Mo alloy catalysts were more active than Pt-alone. Gradual Mo dissolution at the electrode surface was observed after voltammetric and chronoamperometric measurements. The dissolved Mo contributed to the catalytic effect of the electrode as underpotentially deposited (upd) adatoms. This dissolution probably also leads to an increase in the electrode surface roughness. Low molybdenum content in the electrode material enhances the activity toward ethanol oxidation when compared to Pt-alone. Ethanol oxidation was also investigated by *in situ* infrared reflectance spectroscopy in order to determine the presence of adsorbed intermediates like CO species. Acetaldehyde, acetic acid and CO_2 were also found by spectroscopic experiments.

1. Introduction

Ethanol electrooxidation on Pt electrode surfaces is one of the most investigated processes in electrocatalysis [1–5]. Understanding the mechanism and kinetics of this reaction is important for the optimization of fuel cell performance at low temperatures. Ethanol is an attractive substrate because of its various potential applications in transportation and portable electronic devices. Moreover, it is a safe molecule and can be produced on a large scale from biomass. For maximum energy recovery from ethanol it is necessary to achieve its complete oxidation to CO_2 with 12 electrons per molecule. This oxidation requires the C–C bond cleavage and oxidation of intermediate species that adsorb at the sites of Pt electrode [2, 5]. Therefore, modification in catalyst composition is necessary to enhance ethanol electrocatalytic oxidation. Various metals have been studied in several combinations with platinum, resulting in bimetallic catalysts, including alloys. The chemical elements mostly used for this purpose have been Ir, Mo, Os, Ru, Sn, W and Zr [3–14]. Cheaper catalysts can be obtained by using Pt-based catalysts instead of platinum alone. When the second transition metal is more expensive than Pt, its use at low concentration can be justified by the fact that it minimizes the CO poisoning effect. Mo is known for its beneficial cocatalytic effect in CO oxidation and it has also been tested for ethanol oxidation. In previous experiments, the molybdenum cocatalytic effect led to an increase in current densities for small organic compounds [15, 16], but this metal showed no catalytic effect on the initiation of organic molecule oxidation [13, 15–27]. Prior publications studied electrooxidation kinetics of H_2, CO and H_2/CO mixture on smooth and well-characterized Pt–Mo surfaces in 0.5 M H_2SO_4 [6, 7]. These studies suggested that the oxidation states of Mo surface atoms as well as the nature of Mo surface oxides were determining factors in the oxidation of poisoning organic species adsorbed on the Pt surface. It has also been suggested that the Mo oxyhydroxide was reactive toward the oxidative removal of intermediate species like CO. Enhanced activity for methanol oxidation on Pt–MoO_x composite electrodes has been reported by Zhang et al. [28]. This study indicated the possibility of a redox couple involving Mo, the oxidation state changes ascribed to the redox peaks in the voltammogram were a Mo(VI)/Mo(IV) couple. An enhancement in CO tolerance was reported for the Pt–Mo/C (4:1) catalyst, when compared

to Pt/C and the other binary systems tested (Pt–Nb(3:1), Pt–Ta(6:1) and Pt–Ru(E-TEK)) [19]. The inclusion of 10 at % Mo in Pt–Ru resulted in an electrocatalyst with higher activity in the presence of CO when compared to Pt–Ru/C. As can be seen, there are contradictory results according to the method used for the preparation of the catalysts and following the molecule studied. The aim of this work is to investigate the oxidation of ethanol on a Pt modified catalyst by the introduction of a second transition metal. To achieve this purpose, Pt–Mo catalysts with different compositions were prepared by an arc-melting furnace process. Attention was also focused on the behavior of electrodes concerning Mo loss due to their dissolution into the electrolyte, which occurs in some extension according to the Mo content in the Pt-based electrodes.

2. Experimental

The single phase polycrystalline Pt–Mo bimetallic structures, including alloys, were prepared from the pure elements in the required ratios under Ar atmosphere (1.3×10^{-5} bar) in an arc-melting furnace. These compositions were chosen from two different zones of a binary phase diagram where the metals are supposed to form either a pure alloy Pt–Mo (50:50) mixture or a solid solution Pt–Mo (80:20) [25, 27]. In this process, the arc is formed between an electrode and the base plate of a water-cooled copper mold. The temperature reached by this arc is high enough to melt such alloys and the pure elements, which have a high melting point. Six melting cycles were applied to improve the bulk alloy homogeneity. The electrode surface was polished using fine grade paper, followed by alumina powder up to 0.05 μm, until a mirror-finish aspect was obtained. The basic atomic compositions for the bimetallic Pt/Mo alloys were evaluated by Energy Dispersive X-ray Spectroscopy (EDX) analysis, performed in an LEO-440 equipment coupled with a Oxford-7060 model EDX detector containing Si–Li.

A conventional three-electrode electrochemical glass cell was used for cyclic voltammetry. Constant potential chronoamperometry for ethanol oxidation as well as CO-stripping voltammetry was performed on a PC controlled Solartron Potentiostat 1285 Electrochemical Interface. A Reversible Hydrogen Electrode (RHE) and a platinized Pt foil served as reference and counter electrodes, respectively. The working electrodes were electrochemically activated by 25 voltammetric cycles in 0.1 mol L^{-1} H_2SO_4, from 0.05 to 1.5 V vs. RHE. Both the adsorption/desorption hydrogen region and the CO-stripping technique allowed the calculation of the true electrode surface area. All the electrochemical experiments were carried out at room temperature (21 ± 1 °C).

The Fourier transform IR spectrometer was a Nicolet Nexus 670 spectrometer with a MCT detector. The electrochemical cell was fitted with a 60° prismatic CaF_2 and planar ZnSe windows.

3. Results and discussion

EDX analyses of the bimetallic catalysts were performed on different zones of the polished surface samples. Table 1 shows that the determined average atomic compositions of the electrocatalysts are close to the expected values.

CO-stripping voltammograms for Pt–Mo catalysts recorded at room temperature are shown in Figure 1. The electrooxidation of CO starts at lower potentials on Pt–Mo at ca. 0.35 V when the Mo content is 50%.

On the positive-going scan two peaks are observed, which suggests two characteristic oxidation mechanisms, the first at 0.45 V on the surface of Mo (or Mo oxides) and the second, on the Pt–OH sites at ca. 0.7 V. The charge involved in the CO oxidation allowed the determination of the surface areas of the different catalysts (Table 2). The results obtained by the CO pre-adsorbed oxidation were corroborated with those of the integration of the hydrogen region.

Figure 2 shows the cyclic voltammograms of Pt and Pt–Mo bimetallic electrodes in 0.1 mol L^{-1} H_2SO_4 solution. From this figure, it can be seen that the cyclic voltammograms obtained for Pt are well-defined in the support electrolyte. For the Pt–Mo bimetallic electrodes, the steady-state voltammogram recorded after several cycles ($n > 20$) gives evidence of a continuous increase in the peak at 0.45 V/RHE, which is due to the formation

Table 1. Atomic composition of Pt–Mo bimetallic catalysts

Electrocatalyst	Nominal composition/%		Determined by EDX/%	
	Pt	Mo	Pt	Mo
	50	50	52	48
Pt–Mo	80	20	78	22

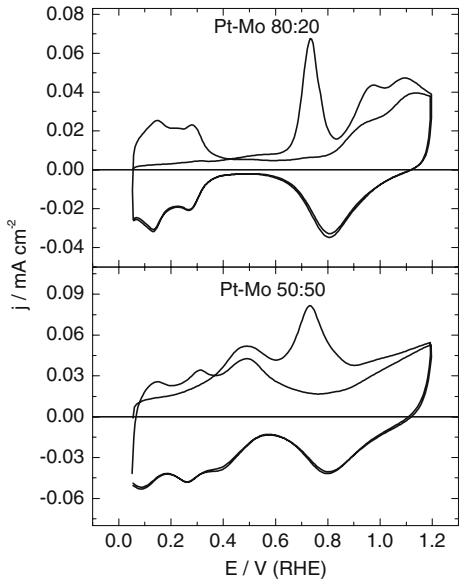

Fig. 1. CO-stripping voltammograms at 21 °C for Pt–Mo bimetallic electrodes in 0.1 mol L^{-1} H_2SO_4 recorded at 50 mV s^{-1}.

Table 2. Estimation of the surface areas of Pt–Mo bimetallic catalysts by CO-stripping and the integration of the hydrogen region

EDX composition	Surface area/cm^2		
	Geometric surface area	H – Desorption	CO_{ads} oxidation
Pt–Mo (78:22)	0.14	0.32	0.37
Pt–Mo (52:48)	0.28	2.75	2.78

of Mo oxides. In the negative-going scan, the reduction peak of Mo species is observed after the peak due to Pt oxides. Its charge is lower than that of the forward peak. This suggests that Mo oxidation involves different oxidation states as follows:

$$Mo^{3+} + 2H_2O = MoO_2 + 4H^+ + e^- \qquad E^\circ = 0.311\ \text{V/SHE} \quad [16] \tag{1}$$

$$MoO_2 + 2H_2O = H_2MoO_{4(aq)} + 2H^+ + 2e^- \qquad E = 0.39\ \text{V/SHE} \quad [29] \tag{2}$$

$$MoO_2 + 2H_2O = HMoO_4^- + 3H^+ + 2e^- \qquad E^\circ = 0.429\ \text{V/SHE} \quad [16, 29] \tag{3}$$

Some Mo soluble species such as H_2MoO_4 can be reduced according to the following equation:

$$H_2MoO_{4(aq)} + 2H^+ + e^- = 2H_2O + MoO_2^+ \qquad E^\circ = 0.4\ \text{V/SHE} \quad [29] \tag{4}$$

However, during the reverse scan the reduction peak due to Mo species is lower in respect of those dissolved in the electrolyte.

Figure 3 shows the positive scan curves in the presence of ethanol. The organic substrate electrooxidation starts at ca. 0.3 V vs. RHE and a decrease in the hydrogen region, due to organic species adsorption is also observed. When compared with pure Pt catalyst, the presence of Mo causes a shift in the ethanol oxidation toward less positive potentials. Mo-modified electrodes remain more active as far as 0.75 V/RHE. After this potential Pt-alone displays higher current densities than Pt–Mo (50:50), which can be understood considering that less Pt–OH sites are available for the oxidative removal of adsorbed CO at this composition. The high activity of Pt–Mo (80:20) is probably due to an increase in the electrode surface roughness caused by dissolution of Mo surface atoms or to an electronic modification of Pt, as reported by Adzic et al. [30, 31].

The performance of catalysts in steady-state conditions during ethanol oxidation were analyzed by chronoamperometric tests (CA) at various potentials (Figure 4). Since at 0.4 V vs. RHE ethanol oxidation occurred concomitantly with the Mo-oxidation process, the CA test was also performed at 0.7 V vs. RHE to avoid the influence of Mo-oxidation. The results shown in Figure 4 are in agreement with those obtained previously from cyclic voltammetry. From 0.4 to 0.5 V vs. RHE, the Pt–Mo (50:50) electrode presented the highest current density value. However, this is an apparent activity toward ethanol oxidation since the contribution from the Mo-oxidation process is taken into account (Figure 2). However, the increase in the electrode potential shows that Pt–Mo (80:20) has the best catalytic performance. The current density profiles clearly show that Pt-based catalysts are more active than Pt alone, since values obtained with the Pt electrode dropped down after about 20 s (Figure 4).

When successive voltammetric measurements were carried out in the supporting electrolyte following those in the presence of ethanol, no changes in the catalyst surfaces were observed. Nevertheless, as reported in the

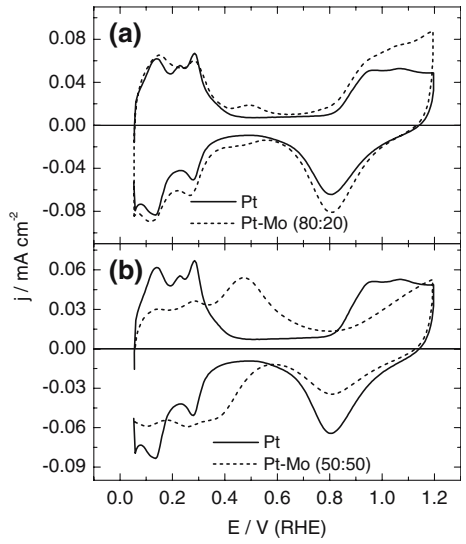

Fig. 2. Cyclic voltammograms of smooth Pt and Pt–Mo bimetallic electrodes in 0.1 mol L^{-1} H_2SO_4 recorded at 50 mV s^{-1}.

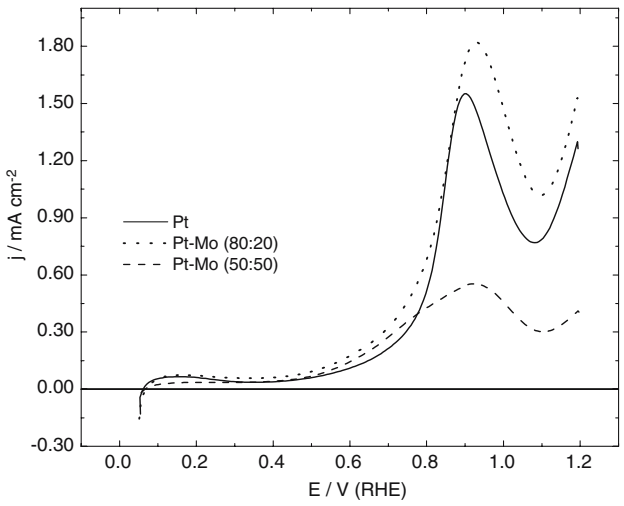

Fig. 3. Anodic sweep curves of Pt and Pt–Mo bimetals in 0.1 mol L^{-1} H_2SO_4 + 0.5 mol L^{-1} C_2H_5OH solutions at a scan rate of 50 mV s^{-1}.

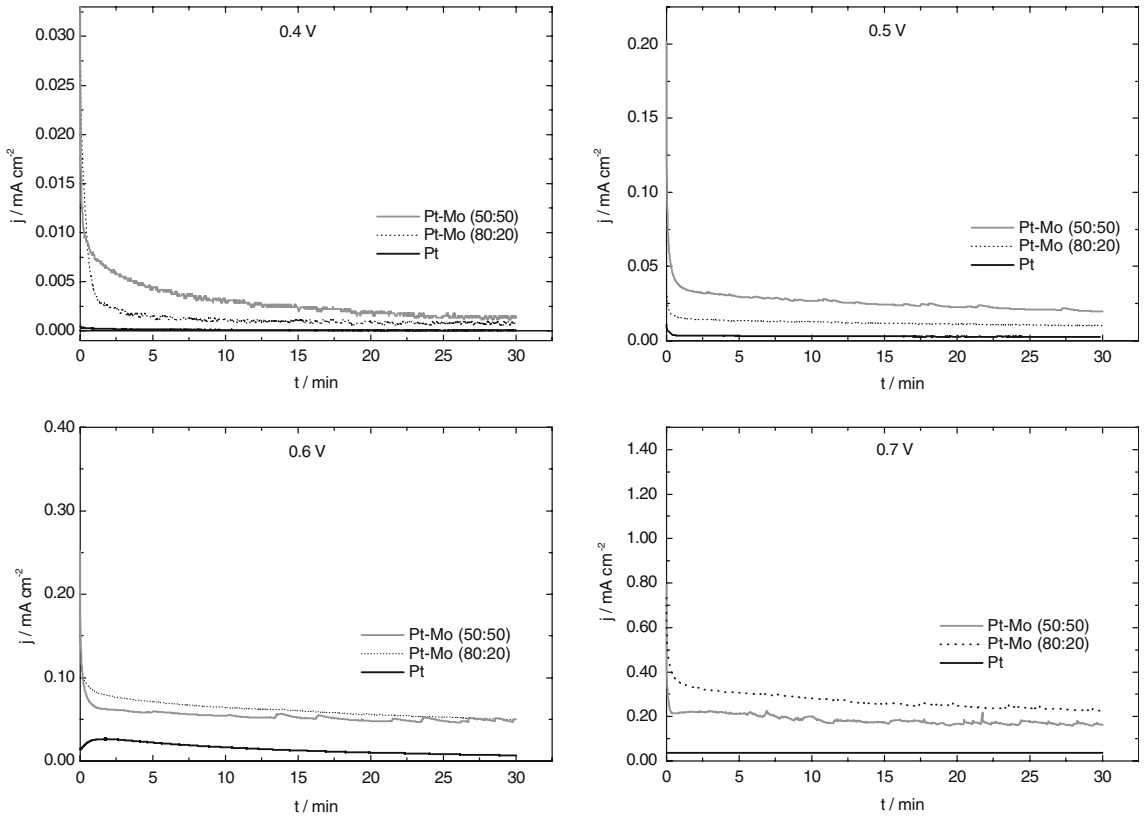

Fig. 4. Potentiostatic oxidations of 0.5 mol L^{-1} C_2H_5OH in 0.1 mol L^{-1} H_2SO_4 on Pt and Pt–Mo bimetallic electrodes for 30 min at various potentials.

literature [13, 25], it is probable that irreversible Mo loss occurs from the electrode surface. Under acidic conditions, the species which best represent the redox couple of dissolved Mo are MoO_3/H_xMoO_3 ($x > 0$). The Mo oxo species present in the solution can re-adsorb at the Pt surface at potentials lower than 0.4 V. Therefore, they behave as underpotentially deposited (upd) adatoms, maintaining the electrode catalytic effect. In order to clarify this point, CV experiments in supporting electrolyte were repeated in a new electrolyte after working in ethanol oxidation. Evolution of the Pt–Mo electrodes voltammetric profiles upon cycling in 0.1 mol L^{-1} H_2SO_4 is shown in Figure 5. Apart from Pt–Mo (50:50) electrode, a gradual decrease in the peaks corresponding to the Mo reduction–oxidation reactions is obvious, suggesting that Mo dissolves into the electrolyte. Quantitative differences in the rate of Mo dissolution become apparent when the cyclic voltammograms recorded at the beginning and those taken after renewing the supporting electrolyte are compared. The increase in the potential as far as 1.5 V in the case of the Pt–Mo (80:20) electrode leads to an oxidation peak at ca. 1.25 V, which must be due to the oxidation of Mo species. To avoid this perturbation of the electrode surface, the anodic potential limit will be set at 1.2 V in the future.

When the Mo composition in the catalyst is 20%, a peak at ca. 0.45 V vs. RHE, typical of the presence of Mo species in the system, disappears in the Pt cyclic voltammogram. At the same time, the adsorption/desorption hydrogen region increases and resembles that of a smooth platinum electrode. As can be seen from the results of Janssen et al. [32, 33], the non-alloyed MoO_3 phase dissolves more rapidly than Mo

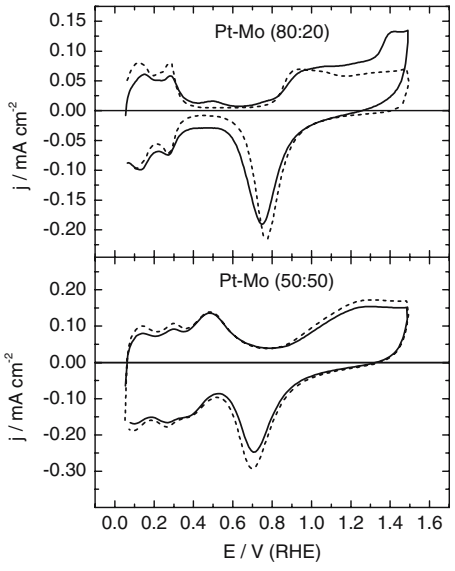

Fig. 5. Cyclic voltammograms of Pt–Mo (50:50) and (80:20) electrodes recorded at a scan rate of 50 mV s^{-1} in 0.1 mol L^{-1} H_2SO_4 before (—) and after (- - -) potentiostatic oxidations of 0.5 mol L^{-1} C_2H_5OH.

from the mixed Pt–MoO_3 phase. These results suggest that an increase in the Mo composition (for example Pt–Mo (50:50)) enhances the relative stability of the catalyst or at least slows down its dissolution by forming a real Pt–Mo alloy, as shown in the binary phase diagram [25, 27].

To confirm the hypothesis that the dissolved Mo continues to promote a catalytic effect for ethanol oxidation, 5×10^{-5} mol L^{-1} of Mo^{5+} from a $MoCl_5$ precursor was added to the supporting electrolyte (Figure 6). In the absence of ethanol, it can be seen that adsorption of Mo-upd decreases the Pt hydrogen adsorption/desorption region, and a quasi reversible redox peak at 0.45 V vs. RHE is also observed (Figure 6(a)). In the presence of ethanol, the Mo-adatoms promote an enhancement in the organic substrate oxidation when compared to the pure Pt catalyst (Figure 6(b)). Figure 6 clearly confirms that dissolved Mo can readsorb at the Pt surface, contributing to an increased electrode performance toward ethanol electrooxidation [13]. According to Adzic et al., the enhanced activity of the catalyst might also signify a fine-tuning of its electronic properties induced by the modification in the Pt monolayer [31].

It is not the purpose of this paper to describe the spectroscopic behavior of ethanol and its products in detail. However, FTIR spectra are very helpful to identify adsorbed species formed before and after the oxidation process. Figure 7 shows FTIR spectra of ethanol adsorption and electrooxidation at the Pt–Mo (50:50) electrode. The reference reflectivity used for the calculation of $\Delta R/R$ was taken at 0.05 V vs. RHE. The band for the linear CO (CO_L) at 2051 cm^{-1} is clearly observed at all potentials, whereas that of CO_2 formation located at 2341 cm^{-1} appears only after potentials higher than 0.5 V vs. RHE. The characteristic adsorption band that is always present at 1630 cm^{-1} is attributed to interfacial water [34–37].

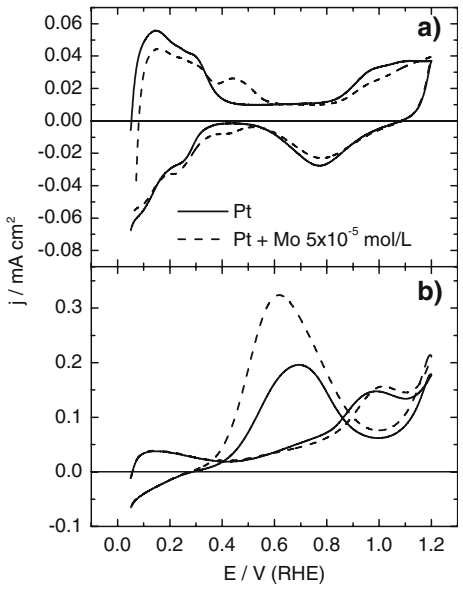

Fig. 6. Cyclic voltammograms of Pt electrode recorded at 50 mV s^{-1} in 0.1 mol L^{-1} H_2SO_4 (a) in the supporting electrolyte; (b) in the presence of 0.5 mol L^{-1} C_2H_5OH + 5.10^{-5}mol L^{-1} Mo^{5+}.

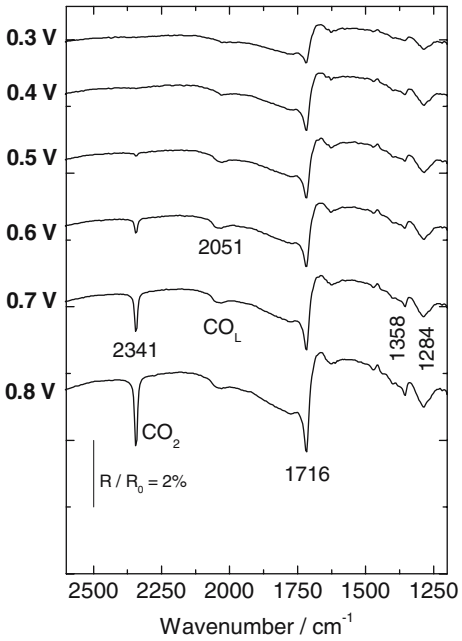

Fig. 7. In situ FTIR spectra of the species resulting from the adsorption and oxidation of 0.5 mol L^{-1} ethanol in 0.1 mol L^{-1} $HClO_4$ on a Pt–Mo (50:50) bimetal at various potentials.

Other absorption bands were observed at around 1716, 1358, and 1284 cm^{-1}. They were respectively attributed to the formation of products containing the carbonyl C = O stretching mode of –COOH or –CHO, a C–O symmetric stretching of adsorbed CH_3COO^-, and a coupled C–O stretching and OH deformation due to –COOH. In order to detect a characteristic band for acetaldehyde, the IR spectra were obtained using a planar ZnSe window as complementary measurements, which allows the detection of IR radiation as low as 800 cm^{-1}. A weak and not well-defined band was detected at 930 cm^{-1}, suggesting that the band at 1716 cm^{-1} is mostly due to acetic acid formation. The bands located between 1280 and 1400 cm^{-1} probably correspond to the symmetric CH_3 bending mode of acetic acid [38, 39].

CO_2 production was followed by IR spectroscopy in the presence of pre-adsorbed CO in order to confirm the efficiency of the Pt–Mo catalyst at modifying the kinetics of the oxidation reaction. Figure 8 shows that CO_{ads} is transformed into CO_2. Comparing the CO_2 profile obtained for the Pt–Mo bimetallic surface with that of Pt-alone shown before [10], two oxidation regions are observed. There is one shoulder between 0.1 and 0.5 V vs. RHE, which is more pronounced for the bimetallic catalyst when compared to results obtained for Pt-alone. The second oxidation takes place at potentials higher than 0.5 V/RHE located at the Pt–OH site domains.

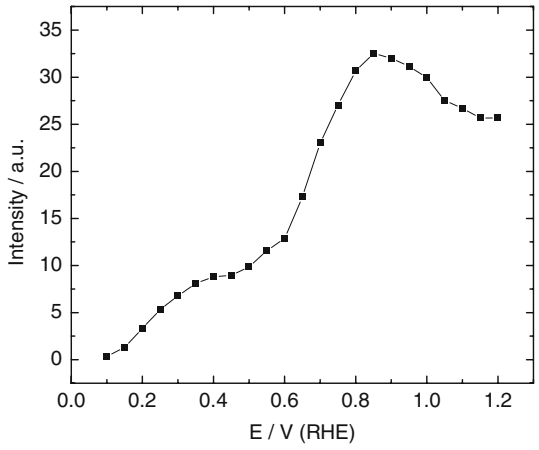

Fig. 8. Intensity of the IR band of CO_2 obtained from the oxidation of pre-adsorbed CO on the Pt–Mo (50:50) electrode.

According to the products detected by *in situ* reflectance spectroscopy, it can be suggested that ethanol adsorbs at the Pt surface, followed by α–C–H dissociation, leading to the formation of adsorbed acetaldehyde:

$$CH_3CH_2OH + Pt \rightarrow Pt(CH_3CH_2OH)_{ads} \quad (5)$$

$$Pt(CH_3CH_2OH)_{ads} \rightarrow Pt(CH_3CHO)_{ads} + 2H^+ + 2e^- \quad (6)$$

$$Pt(CH_3CHO)_{ads} \rightarrow CH_3CHO + Pt \quad (7)$$

Slight CO_{ads} formation observed in Figure 8 at all potentials is evidence that a dissociative C–C bond cleavage occurs through the adsorbed species [37]:

$$Pt(CH_3CHO)_{ads} + Pt \rightarrow Pt(CO)_{ads} + Pt(CH_3)_{ads} + H^+ + e^- \quad (8)$$

Jaksic et al. [25] reported that the highest oxide valence states, in particular MoO_3, block active catalytic centers and decrease the overall catalytic activity. However, lower oxide states (MoO_2, $MoO_2(OH)$) usually exhibit electronic conductivity rather than higher catalytic activity, and spillover to primary oxides (M–OH). Moreover, Mo can activate the interfacial water at lower potentials. With this proposal, ethanol reacts with hydroxyls adsorbed on Mo surface atoms at a low potential range, favoring the formation of acetic acid:

$$H_2O + MO \rightarrow Mo(OH) + H^+ + e^- \quad (9)$$

$$Mo(OH)_{ads} + Pt(CH_3CHO)_{ads} \rightarrow Pt + Mo + CH_3COOH + H^+ + e^- \quad (10)$$

In the potential range above 0.5 V, Mo dissolution combined with the oxidation of the Pt surface also leads to the production of acetic acid, as follows:

$$Pt(CH_3CHO)_{ads} + Pt(OH)_{ads} \rightarrow 2Pt + CH_3COOH + H^+ + e^- \quad (11)$$

As pointed out above, the transformation of acetaldehyde into acetic acid seems to be too fast for acetaldehyde adsorbed species to be detected, although the carboxylic acid can be assigned with the band at 1716 cm^{-1}. IR measurements indicated the presence of CO_2, which is evidence of C–C bond cleavage during the adsorption of ethanol at the electrode surface. This CO_2 absorption band as a final reaction product is located at 2341 cm^{-1} and increases as the potential increases:

$$Pt(CO)_{ads} + Pt(OH)_{ads} \rightarrow 2Pt + CO_2 + H^+ + e^- \quad (12)$$

There is no doubt about the determination of intermediate CO species, which are then oxidized to CO_2 without accumulation at the electrode surface.

4. Conclusions

Pt–Mo anode catalysts were prepared in different compositions to investigate their performance in ethanol electrooxidation. Clear evidence from electrochemical results shows that ethanol oxidation is enhanced on Pt–Mo electrodes when compared with Pt-alone. Voltammetric and chronoamperometric measurements show that this effect increases when the Mo-content decreases in the catalyst composition. Pt–Mo (80:20) exhibited the best performance regarding ethanol oxidation at long term at a steady-state potential. Low Mo content in the catalyst composition leads to fast H_2MoO_4 dissolution from the electrode surface, increasing the electrode roughness. Changes in the surface roughness combined with the behavior of dissolved Mo as upd and the electronic modification in the catalyst monolayer are determining factors which can contribute to a catalytic effect for ethanol electrooxidation. Increasing Mo-content favors the formation of a pure alloy and slows down Mo-dissolution. FTIR spectroscopy measurements helped the determination of the intermediate and final reaction products issued from ethanol oxidation. Bimetallic catalyst favors the cleavage of the C–C bond and the electrooxidation of irreversible adsorbed intermediate species like CO to carbon dioxide.

Acknowledgements

This work was mainly conducted within under the framework of a collaborative programme CAPES/COFECUB (Comité Français d'Evaluation de la Coopération Universitaire avec le Brésil) under grant no 498/05. D. M. dos Anjos thanks CAPES for the Ph-D fellowship. G. Tremiliosi-Filho, P. Olivi and A.R de Andrade acknowledge FAPESP and CNPq for financial support. The authors also acknowledge Roberto B. de Lima for his help in FTIR studies.

References

1. V.P. Santos and G. Tremiliosi-Filho, *J. Electroanal. Chem.* **554** (203) 395.
2. G.A. Camara and T. Iwasita, *J. Electroanal. Chem.* **518** (2005) 315.
3. F. Vigier, C. Coutanceau, F. Hahn, E.M. Belgsir and C. Lamy, *J. Electroanal. Chem.* **563** (2004) 81.
4. C. Lamy, S. Rousseau, E.M. Belgsir, C. Coutanceau and J.-M. Léger, *Electrochim. Acta* **49** (2004) 3901.
5. J.-M. Léger, S. Rousseau, C. Coutanceau, F. Hahn and C. Lamy, *Electrochim. Acta* **50** (2005) 5118.
6. B.N. Grgur, G. Zhuang, N.M. Markovic and P.N. Ross Jr., *J.Phys. Chem. B* **101** (1997) 3910.
7. B.N. Grgur, N.M. Markovic and P.N. Ross Jr., *J. Phys. Chem. B* **102** (1998) 2494.
8. S. Mukerjee and R.C. Urian, *Electrochim. Acta* **47** (2002) 3219.
9. S. Mylswamy, C.Y. Wang, R.S. Liu, J.-F. Lee, M.-J. Tang, J.-J. Lee and B.-J. Weng, *Chem. Phys. Lett.* **412** (2005) 444.
10. J.-M. Léger, *Electrochim. Acta* **50** (2005) 3123.
11. L. Jiang, G. Sun, S. Wang, G. Wang, Q. Xin, Z. Zhou and B. Zhou, *Electrochem. Commun.* **7** (2005) 663.
12. S.Q. Song, W.J. Zhou, Z.H. Zhou, L.H. Jiang, G.Q. Sun, Q. Xin, V. Leontidis, S. Kontou and P. Tsiakaras, *Int. J. Hygrogen Energy* **30** (2005) 995.
13. C. Song, M. Khanfar and P.G. Pickup, *J. Appl. Electrochem.* **36** (2006) 339.
14. Y. Bai, J. Wu, J. Xi, J. Wang, W. Zhu, L. Chen and X. Qiu, *Electrochem. Commun.* **7** (2005) 1087.
15. H. Massong, H. Wang, G. Samjeské and H. Baltruschat, *Electrochim. Acta* **46** (2000) 701.
16. G. Samjeské, H. Wang, Y.T. Löffler and H. Baltruschat, *Electrochim. Acta* **47** (2002) 3681.
17. A.O. Neto, J. Perez, W.T. Napporn, E.A. Ticianelli and E.R. Gonzalez, *J. Braz. Chem. Soc.* **11** (2000) 39.
18. A. Pozio, L. Giorgi, E. Antolini and E. Passalacqua, *Electrochim. Acta* **46** (2000) 555.
19. D.C. Papageorgopoulos, M. Keijzer and F.A. de Bruijn, *Electrochim. Acta* **48** (2002) 197.
20. T. Ioroi, N. Fujiwara, Z. Siroma, K. Yasuda and Y. Miyazaki, *Electrochem. Commun.* **4** (2002) 442.
21. Z. Hou, B. Yi, H. Yu, Z. Lin and H. Zhang, *J. Power Sources* **123** (2003) 116.
22. W.J. Zhou, S.Q. Song, W.Z. Li, Z.H. Zhou, G.Q. Sun, Q. Xin, S. Douvartzides and P. Tsiakaras, *J. Power Sources* **140** (2003) 50.
23. E.I. Santiago, G.A. Camara and E.A. Ticianelli, *Electrochim. Acta* **48** (2003) 3527.
24. W.J. Zhou, S.Q. Song, W.Z. Li, G.Q. Sun, Q. Xin, S. Kontou, K. Poulianitis and P. Tsiakaras, *Solid State Ionics* **175** (2004) 797.
25. J.M. Jaksic, Lj. Vracar, S.G. Neophytides, S. Zafeiratos, G. Papakonstantinou, N.V. Krstajic and M.M. Jaksic, *Surf. Sci.* **598** (2005) 156.
26. S. Mukerjee, S.L. Lee, E.A. Ticianelli, J. McBreen, B.N. Grgur, N.M. Markovic, P.N. Ross, J.R. Giallombardo and E.S. de Castro, *Electrochem. Solid State Lett.* **2** (1999) 12.
27. M.M. Jaksic, *Electrochim. Acta* **45** (2000) 4085.
28. J. Zhang, Y. Wang, E.R. Fachini and C.R. Cabrera, *Electrochem. Solid State Lett.* **2** (1999) 437.
29. A.J. Bard, R. Parsons and J. Jordan, *in* M. Dekker (ed.), *Aqueous Solution*, (IUPAC, New York and Basel, 1985), p. 453.
30. K. Sasaki, Y. Mo, J.X. Wang, M. Balasubramanian, F. Uribe, J. McBreen and R.R. Adzic, *Electrochim. Acta* **48** (2003) 3841.
31. J. Zhang, F.H.B. Lima, M.H. Shao, K. Sasaki, J.X. Wang, J. Hanson and R.R Adzic, *J. Phys. Chem. B* **109** (2005) 22701.
32. N.P Lebedeva and G.J.M. Janssen, *Electrochim. Acta* **51** (2005) 29.
33. G.J.M. Janssen, *J. Power Sources* **136** (2004) 45.
34. T. Iwasita and E. Pastor, *Electrochim. Acta* **39** (1994) 531.
35. S.C. Chang, L.W. Leung and M.J. Weaver, *J. Phys. Chem.* **94** (1990) 6013.
36. T. Iwasita, B. Rasch, E. Cattaneo and W. Vielstich, *Electrochim. Acta* **34** (1989) 1073.
37. J.M. Perez, B. Beden, F. Hahn, A. Aldaz and C. Lamy, *J. Electroanal. Chem.* **262** (1989) 251.
38. A. Rodes, E. Pastor and T. Iwasita, *J. Electroanal. Chem.* **376** (1994) 10.
39. M.H. Shao and R.R Adzic, *Electrochim. Acta* **50** (2005) 2415.